Valence-band parameters and g factors of ZnTe from free-exciton magnetoreflectance

H. Venghaus* and B. Jusserand†
Max-Planck-Institut für Festkörperforschung, D 7 Stuttgart 80, Federal Republic of Germany
(Received 21 January 1980)

Reflectance of the 1S free-exciton states is measured on ZnTe in magnetic fields up to 18 tesla on polished (100) and cleaved (110) surfaces. Transverse eigenenergies are determined by a line-shape fit. The analysis of the magnetic-field-induced shift and splitting of the exciton subcomponents is based on existing low-field theories with a modification of diamagnetic terms. They are reduced according to a two-band model variational calculation valid for polar materials up to $\gamma \simeq 1$. We derive valence-band parameters γ_2 and γ_3 from the anisotropy of the σ- and π-polarized transitions observed for different orientation of the magnetic field. We further evaluate the exciton reduced mass μ_0 from the exciton Rydberg energy and determine g factors from the observed linear Zeeman splitting. Renormalized (polaron) parameters derived are: $\mu_0^*/m_0 = 0.080 \pm 0.005$, $\gamma_1^* = 3.9 \pm 0.7$, $\gamma_2^* = 0.83 \pm 0.08$, and $\gamma_3^* = 1.30 \pm 0.12$, corresponding to bare parameters $\mu_0/m_0 = 0.074 \pm 0.005$, $\gamma_1 = 4.4 \pm 0.7$, $\gamma_2 = 0.95 \pm 0.09$, and $\gamma_3 = 1.48 \pm 0.14$, respectively. We further derive an electron g factor $g_c = -0.6 \pm 0.3$, an effective-hole g factor $\tilde{\kappa} = -0.1 \pm 0.1$, and an anisotropic-hole g value $\tilde{q} = -0.02$. For $\vec{B} \| [110]$, Voigt configuration, and π polarization we observe a mixing between dipole-allowed and dipole-forbidden states, which results in the observability of a third transition compared to two transitions observed for $\vec{B} \| [100]$.

I. INTRODUCTION

Magneto-optical experiments on free-exciton states in semiconductors are carried out for various reasons. Examples are the derivation of fundamental material parameters, the test of theoretical models on the basis of parameters already known, or the investigation of particular effects such as the short-range electron-hole spin-exchange interaction or k-linear term induced mixing of different exciton subcomponents.[1,2]

In the present paper we investigate the free exciton of ZnTe by normal-incidence magnetoreflectance measurements in magnetic fields up to 18 T, and the main purpose is the derivation of g factors and valence-band parameters. The latter are of great interest for the theoretical description of acceptor states in ZnTe, which are currently under investigation in considerable detail.[3,4]

Derivation of valence-band parameters γ_i from free-exciton magnetoreflectance data requires the availability of an appropriate theory. To be suited for an analysis of the present data such a theory must be valid for (i) degenerate valence bands, (ii) magnetic fields up to $\gamma \lesssim 1$ [cf. Eq. (3.1c)], and (iii) polar materials. Unfortunately, a theory which simultaneously meets requirements (i)–(iii) does not exist at present. The perturbational theory of Cho *et al.*[5] which is an extension of earlier work by Altarelli and Lipari[6] is valid for degenerate valence bands, but only up to $\gamma \lesssim 0.4$ and for nonpolar materials. The variational calculation of Behnke *et al.*[7] is valid for $\gamma \lesssim 1$ and polar materials, but does not take into account a degenerate valence band. Ekardt's theory of excitons in zinc-blende-structure semiconductors in intermediate magnetic fields[8] does not take into account polaron effects, and it is restricted to $\gamma \gtrsim 1$ owing to numerical difficulties.

It turns out that Cho's theoretical treatment[5] is the most appropriate basis for the analysis of the present experiments. The linear Zeeman splitting between the main σ^+- and σ^--polarized transitions is determined in the range $0 < \gamma < 0.4$, and the results also represent the experimental data up to $\gamma = 1$. We also do not observe any indication for deviations from linear splitting between the (main) π-polarized states; thus there is no problem in applying Cho's theory up to $\gamma = 1$ as far as the linear Zeeman splitting is concerned. This is in contrast to similar experiments on InP and GaAs, where such deviations are already observed for $\gamma \gtrsim 0.6$.[9]

Problems arise with respect to quadratic terms for $\gamma \gtrsim 0.4$. Compared to the low-field formula the exciton diamagnetic shift is reduced as γ approaches 1 (Ref. 10), and the shift is further reduced in polar materials.[7] We determine this reduction in an exact variational calculation in a two-band model and assume that the same relative reduction is appropriate for degenerate valence bands. This extends the applicability range of Ref. 5 to the present experimental situation.

Justification of our approach is provided by comparison between experiment and theory. Our procedure excludes the possibility of determining the exciton reduced mass μ_0 from the diamagnetic shift, which depends essentially on μ_0. Thus we derive the exciton reduced mass μ_0 from the ex-

citon Rydberg energy R_0. With respect to diamagnetic terms depending on γ_2 and γ_3 we assume that they are reduced in the same way as the mean diamagnetic shift rate.

Possible errors due to this assumption are expected to be reduced by deriving γ_2 and γ_3 from expressions which are independent of the mean diamagnetic shift rate. Our theoretical approach and the results obtained are supported by the following: (1) We get a good representation of the overall exciton splitting pattern; (2) the valence-band parameters derived here give a good representation of shallow acceptor states[3] observed by other experiments (cf. Sec. V).

The paper is organized as follows: After a brief summary of experimental details in Sec. II, we compile in Sec. III the results of the low-field theory of Γ_6-Γ_8 exciton states, which are relevant for the analysis of our data. Experimental results are given in Sec. IV, starting with the electron and hole g values, followed by the free-exciton reduced mass and the valence-band parameters γ_i. The results obtained here are discussed and compared to the results of other authors in Sec. V.

II. EXPERIMENTAL

ZnTe crystals used in the present investigation were grown by a modified Bridgman technique in a carbon-lined quartz ampoule under Te-rich conditions at 1100 °C.[11] The crystals were either not intentionally doped or P doped with acceptor concentrations in the $10^{16}/\mathrm{cm}^3$ range. Experiments were performed both on polished (100) and cleaved (110) surfaces. The (100) faces were mechanically polished and etched with Br-methanol of increasing dilution.

The crystals were mounted strain-free in a helium flow exchange gas cryostat and cooled down to ~4 K. Reflectance was measured with a quartz-iodine lamp and a conventional optical system. The detection system consisted of a $\frac{3}{4}$-m single grating monochromator, a photomultiplier tube, and a lock-in amplifier or a photon-counting set-up. The magnetic field was produced by a 12.8 T superconducting magnet or alternatively by a 10-MW 20-T Bitter-type magnet.

III. THEORY

A. Line-shape analysis

Analysis of the experimental data and comparison with theoretical calculations requires the determination of transverse eigenenergies of the various exciton sublevels. In the present investigation these energies are derived from the experimentally observed spectra by means of a line-shape fit. If *two* transitions are observed for a given polarization, theoretical reflectance curves are calculated from a dielectric function with two resonances including spatial dispersion as outlined in detail in Refs. 12 and 13. The wave vectors corresponding to the three transverse modes propagating in the crystal are obtained from an equation cubic in $\vec{k}^2$, where $\vec{k}$ represents the wave vector. For the case of *three* nearby transitions theoretical reflectance curves are calculated from a dielectric function with three resonances but *without* spatial dispersion. Taking into account spatial dispersion for the case of three oscillators requires the solution of an equation of fourth order in $\vec{k}^2$ and would lead to considerable numerical problems. Our simplification is justified by the following fact: If only two oscillators are observed we obtain within experimental accuracy the same results concerning energy separation and relative strength of the two oscillators from a line-shape fit which either includes or neglects spatial dispersion.

B. General considerations and definitions

The magnetic-field-induced splitting and shift of exciton subcomponents will be discussed on the basis of the low-field theory as outlined in Ref. 5. If not otherwise stated all definitions in the present paper are as given in Ref. 5. However, differing from Ref. 5, we will use $|m_j\rangle\alpha$, $|m_j\rangle\beta$ basis functions, which appear more convenient than the $J=1$, $J=2$ basis, if the electron-hole spin exchange can be neglected. In the present case this assumption is justified, since the analysis is based on experimental data, where the Zeeman splitting is significantly larger than the upper limit for the spin exchange $|\tilde{\Delta}_1|$. α and β are the usual spin functions characterizing Γ_6 conduction-band levels. States of the Γ_8 ($J=\frac{3}{2}$) valence band are represented by $|m_j\rangle$ where $m_j=\pm\frac{1}{2},\pm\frac{3}{2}$.

For our analysis and discussion the following definitions are relevant:

$$R_0=\mu_0 e^4/2\hbar^2\epsilon^2\,, \tag{3.1a}$$

$$1/\mu_0=1/m_e+\gamma_1/m_0\,, \tag{3.1b}$$

$$\gamma=e\hbar H/2\mu_0 cR_0\,, \tag{3.1c}$$

$$\tilde{\kappa}=\kappa-d-\tfrac{13}{6}d(\tau-1)+\tfrac{7}{6}f\,, \tag{3.1d}$$

$$\tilde{q}=q+\tfrac{2}{3}d(\tau-1)-\tfrac{2}{3}f\,, \tag{3.1e}$$

$$d=1.798(\mu_0/m_0)\gamma_3^2\,, \tag{3.1f}$$

$$\tau=\gamma_2/\gamma_3\,, \tag{3.1g}$$

$$\nu=2.268(\mu_0\gamma_2/m_0)^2(2+3/\tau^2)\,, \tag{3.1h}$$

$$\delta'=1.767\mu_0\gamma_2/m_0\,, \tag{3.1i}$$

$$\sigma'=1.688(\mu_0 a_0 K_1/\hbar)^2\,, \tag{3.1k}$$

$$\bar{c}_2=\tfrac{1}{2}\gamma^2 R_0\delta'\,, \tag{3.1l}$$

$$\bar{c}_3=\tfrac{1}{2}\gamma^2 R_0 2[\delta'(1/\tau-1)+\sigma']\,, \tag{3.1m}$$

$$\bar{\kappa}=\tilde{\kappa}\mu_B H;\quad \bar{q}=\tilde{q}\mu_B H;\quad \bar{g}_c=g_c\mu_B H\,. \tag{3.1n}$$

ϵ is the effective (static) dielectric constant, which has to be distinguished from the background dielectric constant ϵ_b, used in the calculation of theoretical reflectance spectra. a_0 is the exciton Bohr radius, K_1 the coefficient of the k-linear term and f is a small correction depending on K_1^2 (cf. Ref. 5). All other symbols have their usual meaning.

Renormalized (polaron) valence-band parameters are marked with an asterisk (*) in the following, bare parameters are unlabeled. The relation between bare and renormalized valence-band parameters is given, for example, in Ref. 14. The asterisk is omitted in expressions which hold equally for polar and nonpolar materials and where no distinction is made between renormalized and bare parameters. The asterisk also distinguishes the renormalized electron mass from the bare conduction band electron mass.

We extend the applicability range of Ref. 5 in the following way: We determine the exciton diamagnetic shift $\Delta E^*_{\rm dia}$ in a two-band model variational calculation according to Ref. 7. By comparison with the low-field-limit hydrogenic diamagnetic shift we define a correction function $F^*(\gamma)$ according to

$$F^*(\gamma)=\Delta E^*_{\rm dia}(\gamma)/\tfrac{1}{2}\gamma^2 R_0 \tag{3.2}$$

and multiply all diamagnetic terms in Ref. 5, which are valid for degenerate valence bands, by $F^*(\gamma)$.

Alternatively, we calculate the diamagnetic shift rate according to Ref. 5 using *renormalized* input parameters to take into account polaron effects. To get results valid for $\gamma\lesssim 1$ we further correct the diamagnetic shift according to Ref. 10. The results obtained in this way are practically the same (less than 3% deviation) as calculated from the *bare* parameters and correcting with the function $F^*(\gamma)$ [Eq. (3.2)].

C. Electron and hole effective g factors

The Zeeman splitting observed between various exciton sublevels and for different orientations of the magnetic field can be used to derive the electron and hole g factors, g_c and $\tilde{\kappa}$, respectively, and also the parameter $\tilde{q}$, which characterizes the nonspherical contributions to $\tilde{\kappa}$.

The predominant transitions observed in Faraday configuration and σ^+- and σ^--polarization are the $|\tfrac{3}{2}\rangle\beta$ and $|-\tfrac{3}{2}\rangle\alpha$ states, respectively. The energy separation between these two states for $\vec{B}\parallel[hkl]$ is characterized by the g factor $g_{\sigma,hkl}$, which is defined by

$$E(|-\tfrac{3}{2}\rangle\alpha)-E(|\tfrac{3}{2}\rangle\beta)=g_{\sigma,hkl}\mu_B H \quad \text{for } \vec{B}\parallel[hkl], \tag{3.3}$$

In Voigt configuration and π polarization the predominant states are $|\tfrac{1}{2}\rangle\beta$ and $|-\tfrac{1}{2}\rangle\alpha$. Analogous to Eq. (3.3) we define $g_{\pi,hkl}$ by

$$E(|-\tfrac{1}{2}\rangle\alpha)-E(|\tfrac{1}{2}\rangle\beta)=g_{\pi,hkl}\mu_B H \quad \text{for } \vec{B}\parallel[hkl]. \tag{3.4}$$

Explicit expressions for $g_{i,hkl}$ can be taken from Ref. 5. For our analysis the following g factors are relevant:

$$g_{\sigma,100}=6\tilde{\kappa}+g_c+\tfrac{27}{2}\tilde{q}\,, \tag{3.5}$$

$$g_{\pi,100}=2\tilde{\kappa}+g_c+\tfrac{1}{2}\tilde{q}\,, \tag{3.6}$$

$$g_{\pi,111}=2\tilde{\kappa}+g_c+\tfrac{13}{2}\tilde{q}\,, \tag{3.7}$$

For $\vec{B}\parallel[100]$ or for any orientation within the spherical model two states are observable for σ^+ polarization (viz. $|\tfrac{3}{2}\rangle\beta$ and $|\tfrac{1}{2}\rangle\alpha$) and also for σ^- polarization (viz. $|-\tfrac{3}{2}\rangle\alpha$ and $|-\tfrac{1}{2}\rangle\beta$). The energy separation between these two states is given for $\vec{B}\parallel[100]$ by

$$E(|\tfrac{3}{2}\rangle\beta)-E(|\tfrac{1}{2}\rangle\alpha)=-g_{\pi,111}\mu_B H+2\bar{c}_2\quad(\sigma^+)\,, \tag{3.8}$$

$$E(|-\tfrac{3}{2}\rangle\alpha)-E(|-\tfrac{1}{2}\rangle\beta)=g_{\pi,111}\mu_B H+2\bar{c}_2\quad(\sigma^-)\,. \tag{3.9}$$

For $\vec{B}\parallel[110]$ simple expressions similar to Eqs. (3.5), (3.6), and (3.7) cannot be given, owing to the mixing between the $|\tfrac{3}{2}\rangle$ and $|-\tfrac{1}{2}\rangle$ and that between the $|-\tfrac{3}{2}\rangle$ and $|\tfrac{1}{2}\rangle$ valence-band states. In this case the analysis requires diagonalization of the following matrix:

$$
\begin{array}{cccc}
\left|\tfrac{3}{2}\right\rangle\alpha & \left|-\tfrac{1}{2}\right\rangle\alpha & \left|-\tfrac{3}{2}\right\rangle\beta & \left|\tfrac{1}{2}\right\rangle\beta \\
\left|\tfrac{3}{2}\right\rangle\beta & \left|-\tfrac{1}{2}\right\rangle\beta & \left|-\tfrac{3}{2}\right\rangle\alpha & \left|\tfrac{1}{2}\right\rangle\alpha
\end{array}
$$

$$
\begin{pmatrix}
-3\bar{\kappa}\pm\frac{1}{2}\bar{g}_c+\bar{c}_2-6\bar{q}+\frac{3}{8}\bar{c}_3 & -(\sqrt{3}/8)(6\bar{q}+\bar{c}_3) & 0 & 0 \\
-(\sqrt{3}/8)(6\bar{q}+\bar{c}_3) & \bar{\kappa}\pm\frac{1}{2}\bar{g}_c-\bar{c}_2+\frac{5}{2}\bar{q}-\frac{3}{8}\bar{c}_3 & 0 & 0 \\
0 & 0 & 3\bar{\kappa}\mp\frac{1}{2}\bar{g}_c+\bar{c}_2+6\bar{q}+\frac{3}{8}\bar{c}_3 & (\sqrt{3}/8)(6\bar{q}-\bar{c}_3) \\
0 & 0 & (\sqrt{3}/8)(6\bar{q}-\bar{c}_3) & -\bar{\kappa}\mp\frac{1}{2}\bar{g}_c-\bar{c}_2-\frac{5}{2}\bar{q}-\frac{3}{8}\bar{c}_3
\end{pmatrix}. \tag{3.10}
$$

The upper (lower) signs in Eq. (3.10) correspond to the upper (lower) set of basis functions, given above the matrix. Owing to the nonzero off-diagonal elements four states are in principle observable for σ^+, σ^-, and π polarization, respectively. Whether more than two states are actually observed at higher magnetic fields depends on the relative magnitude of the off-diagonal elements compared to the difference between the corresponding diagonal elements. In the present case we observe three states for Voigt configuration and π polarization (cf. Sec. IV B), but two states for σ^+ and σ^- polarization in Faraday configuration.

D. Valence-band parameters γ_i

The valence-band parameter γ_1 can be derived from an analysis of free-exciton states in an indirect way only. The experiments yield the exciton reduced mass μ_0, and γ_1 can be calculated from μ_0 provided the electron effective mass m_e is known. The experimental error of γ_1 derived in this way is generally large in direct gap materials, where m_e is small, and thus $1/m_e$ is considerably larger than γ_1.

The exciton reduced mass μ_0 may either be derived from the free-exciton (FE) Rydberg energy or from the mean diamagnetic shift rate of the exciton sublevels. Since a rigorous theory of diamagnetic shift rates in polar materials with valence-band degeneracy is lacking we choose the former alternative.

The valence-band parameters γ_2 and γ_3 can be derived from experimentally determined quantities which are independent of the mean diamagnetic shift rate. The difference between the diamagnetic shift observed for $\vec{B}\parallel[110]$ and that observed for $\vec{B}\parallel[100]$ can be used to determine the ratio γ_3/γ_2 according to (cf. Ref. 5)

$$
[\Delta E^{-}_{\mathrm{dia}}(110)-\Delta E^{-}_{\mathrm{dia}}(100)]/\Delta E^{-}_{\mathrm{dia}}(100) = \tfrac{3}{4}(\gamma_3/\gamma_2-1+\sigma'/\delta'), \tag{3.11}
$$

where $\Delta E^{-}_{\mathrm{dia}}(hkl)=\Delta E^{\sigma}_{\mathrm{dia}}-\Delta E^{\pi}_{\mathrm{dia}}$ for $\vec{B}\parallel[hkl]$, $\Delta E^{\sigma}_{\mathrm{dia}}$ is the average diamagnetic shift of the σ-polarized $\left|-\tfrac{3}{2}\right\rangle\alpha$ and $\left|\tfrac{3}{2}\right\rangle\beta$ states observed in Faraday configuration and $\Delta E^{\pi}_{\mathrm{dia}}$ is the shift of the $\left|-\tfrac{1}{2}\right\rangle\alpha$ and $\left|\tfrac{1}{2}\right\rangle\beta$ states observable in Voigt configuration for π polarization. Expression (3.11) is derived neglecting the off-diagonal mixing between the $\left|-\tfrac{3}{2}\right\rangle$ and $\left|\tfrac{1}{2}\right\rangle$ and that between the $\left|\tfrac{3}{2}\right\rangle$ and $\left|-\tfrac{1}{2}\right\rangle$ valence-band states.

The valence-band parameter γ_2 measures the difference between light- and heavy-hole masses and a nonzero γ_2 induces a difference between the diamagnetic shift rates $\Delta E^{\sigma}_{\mathrm{dia}}$ and $\Delta E^{\pi}_{\mathrm{dia}}$. γ_2 can be derived from this difference according to (cf. Ref. 5)

$$
(\Delta E^{\sigma}_{\mathrm{dia}}-\Delta E^{\pi}_{\mathrm{dia}})/(\Delta E^{\sigma}_{\mathrm{dia}}+\Delta E^{\pi}_{\mathrm{dia}})=\delta'/(1-\nu). \tag{3.12}
$$

Inserting the numerical value for γ_3/γ_2 determined previously transforms Eq. (3.12) into a quadratic equation for the determination of $(\mu_0\gamma_2)$. From $(\mu_0\gamma_2)$ the parameter γ_2 is immediately obtained, if μ_0 was determined previously.

IV. RESULTS

A. Electron-hole spin-exchange interaction

Our spectra are analyzed assuming negligible short-range electron-hole spin exchange $\tilde{\Delta}_1$, since within our experimental accuracy we did not observe any clear indication for finite $\tilde{\Delta}_1$. In the spherical model and also for $\vec{B}\parallel[100]$ orientation two transitions are dipole allowed for σ^+, σ^-, and π polarization, respectively. Two transitions are also allowed for $\vec{B}\parallel[111]$ and π polarization. Without electron-hole spin exchange the relative intensities are 3:1 for the σ^+- and σ^--polarized transitions and 1:1 for the π-polarized transitions. These intensity ratios change if the electron-hole spin-exchange energy becomes comparable to the Zeeman splitting of the two transitions for a given polarization.[15] The π-polarized spectra are always represented best assuming 1:1 relative intensity for the two oscillators, i.e., negligible spin-exchange energy. With respect to the σ-polarized spectra the experiments are less conclusive. For σ^- polarization the two transitions are close together and a single reflectance structure is observed even at 18 T. Two transitions are observed for

σ^+ polarization, and in a considerable number of spectra the lower-energy reflectance structure was less pronounced than expected for 1:3 relative intensity ratio. However, within our experimental accuracy this does not really prove nonzero $\tilde{\Delta}_1$ since the relative intensity is apparently dependent on the sample surface conditions. Thus we assume $\tilde{\Delta}_1 = 0$, although our experiments only suggest $|2\tilde{\Delta}_1| \lesssim 0.1$ meV. This is in agreement with $|2\tilde{\Delta}_1| \lesssim 0.01$ meV reported in Ref. 16, while our experiments do not support $|2\tilde{\Delta}_1| = 0.28$ meV as given in Ref. 17.

B. Electron and hole g factors

Experimental results for Voigt configuration and π polarization are shown in Fig. 1 for $B = 12$ and 18 T. The spectra were taken for $\vec{B} \parallel [111]$. The broken curves are calculated including spatial dispersion; the dotted curves are obtained neglecting spatial dispersion. The parameters used for the calculation are relative intensity for the two oscillators 1:1, background dielectric constant $\epsilon_b = 9.9$. This value is obtained from Ref. 18 by extrapolating the data to the free-exciton energy and assuming ϵ_b to be smaller by 0.3 at 4 K as compared to room temperature according to Ref. 19. We further use a zero magnetic field oscillator strength $4\pi\beta$ (0 T) $= 5\times10^{-3}$, corresponding to 0.6 meV longitudinal-transverse (LT) splitting. This value is derived from a best fit to the experimentally determined reflectance curves for $0 \leq B \leq 18$ T. The dependence of β on the magnetic field strength is calculated according to Ref. 10. For $B = 18$ T we obtain $4\pi\beta\,(18\text{ T}) = 6.7\times10^{-3}$. In the calculation including spatial dispersion we further use a translational exciton mass $M_{111} = 0.47 m_0$ calculated according to Ref. 20, an empirical damping constant $\Gamma = 0.25$ meV, and an 80-Å exciton-free layer. For the calculation neglecting spatial dispersion we use $\Gamma = 0.6$ meV and a 120-Å exciton-free layer. We do not attribute significance to the difference between an 80 and a 120 Å exciton-free layer, since the assumption of a sudden change from a surface layer without excitons to the bulk is a first approximation anyway.[15]

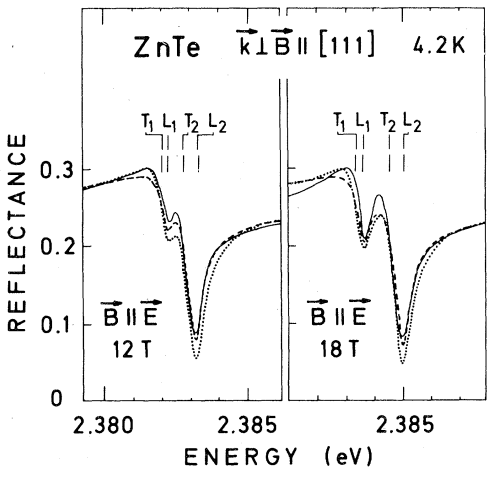

FIG. 1. Normal-incidence reflectance in Voigt configuration and π polarization for $\vec{B} \parallel [111]$, $B = 12$, 18 T. Solid lines: experimental spectra. Broken lines: theoretical calculation *including* spatial dispersion (SD). Dotted lines: theoretical calculation *neglecting* SD. T, L: energies of transverse and longitudinal exciton states. Upper labels (T_i, L_i) refer to spectra including SD, lower labels obtained without SD. Absolute reflectance calculated, not measured. 1:1 relative oscillator strengths, other parameters see text.

The overall agreement between experiment and theory is slightly better if spatial dispersion is taken into account. The energy separation between the transverse eigenenergies determined in both cases is almost the same (cf. Figs. 1 and 3, below), and compared to the experimental error the difference is insignificant. This result justifies the neglect of spatial dispersion in the analysis of spectra which exhibit three oscillators.

A reliable determination of the Zeeman splitting observed in Voigt configuration for π polarization could be made for $B \geq 10$ T only. For lower magnetic fields the second (low-energy) reflectance structure is not sufficiently pronounced. We observe a linear dependence of the splitting on magnetic field strength which is proportional to B up to 18 T and we derive

$$g_{\pi,111} = 2\tilde{\kappa} + g_c + \tfrac{13}{2}\tilde{q} = -1.1 \pm 0.1\,. \tag{4.1}$$

Reflectance spectra taken for $\vec{B} \parallel [100]$, Voigt configuration and π polarization are qualitatively the same as for $\vec{B} \parallel [111]$. The g factor derived in this case is

$$g_{\pi,100} = 2\tilde{\kappa} + g_c + \tfrac{1}{2}\tilde{q} = -0.9 \pm 0.1\,. \tag{4.2}$$

The sign of g_π is determined according to Eqs. (3.8) and (3.9). In ZnTe the energy separation between the $|\tfrac{3}{2}\rangle\beta$ and $|\tfrac{1}{2}\rangle\alpha$ states is larger than that between the $|-\tfrac{3}{2}\rangle\alpha$ and $|-\tfrac{1}{2}\rangle\beta$ states (the latter could not be observed even at 18 T). For this reason $g_\pi < 0$ taking into account that $\bar{c}_2$ is always positive.

The Zeeman splitting between the $|\tfrac{3}{2}\rangle\beta$ and $|-\tfrac{3}{2}\rangle\alpha$ levels yields the g factor g_σ [cf. Eqs. (3.3), (3.5), and (3.6)]. We derived g_σ from the simultaneously measured sum and difference of the σ^+- and σ^--polarized reflectance for $B \leq 7$ T. The quantity immediately obtained is the splitting

$\Delta E'$ between the σ^+- and σ^--polarized reflectance *minima*, where $\Delta E' = g'_\sigma \mu_B H$. The experimentally observed magnitude of g'_σ becomes larger as B increases and remains constant for $B > 5$ T. We observe

$$g'_{\sigma,100} = -1.0 \quad \text{at } B = 1 \text{ T}, \tag{4.3}$$

$$g'_{\sigma,100} = -1.15 \quad \text{for } B > 5 \text{ T}. \tag{4.4}$$

This change of g'_σ is attributed to the fact that the σ^+- and σ^--polarized reflectance structures are both due to *two* oscillators, although one structure is observed only for a given polarization in the range of magnetic fields under consideration here. Figure 2 explains the effect (cf. also Ref. 12). The curves labeled L_1, L_2 show the energy of the longitudinal eigenstates of two nearby oscillators as a function of oscillator separation. If the energy separation between the two oscillators is small compared to the LT splitting Δ_{LT} (as in the case discussed here), a single reflectance minimum corresponding to L_2 is observed. (If spatial dispersion is taken into account the energy of the reflectance minimum does not coincide exactly with L_2; however, this does not affect our conclusions.) The energy separation determined experimentally is that between L_2 for σ^+ polarization and L_2 for σ^- polarization, $L_2(\sigma^+)$ and $L_2(\sigma^-)$, and the curvature of the L_2 curves gives rise to the changes observed for g'_σ. The actually measured change of g'_σ depends on the relative ordering of the σ^+- and σ^--polarized states and on the splitting between the two oscillators for a given polarization. In the present case the splitting between the σ^+-polarized states is larger than that between the σ^--polarized transitions, and $L_2(\sigma^+)$ is at higher energy than $L_2(\sigma^-)$. Contributions of quadratic terms to the splitting between T_1 and T_2 for a given polarization are negligible at small magnetic fields.

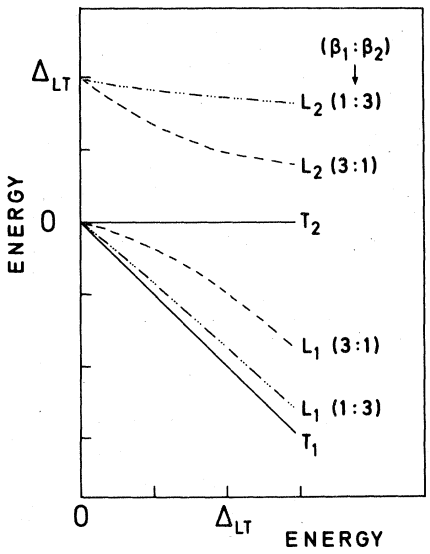

FIG. 2. Longitudinal exciton states (L_1, L_2) as a function of energy separation between transverse exciton states T_1 and T_2 for 1:3 and 3:1 relative oscillator strengths of the two oscillators.

The g factor g_σ which represents the splitting between the $|\frac{3}{2}\rangle\beta$ and $|-\frac{3}{2}\rangle\alpha$ states and which we derive from the observed splitting between the reflectance minima is

$$g_{\sigma,100} = 6\tilde{\kappa} + g_c + \tfrac{27}{2}\tilde{q} = -1.5 \pm 0.2\,. \tag{4.5}$$

For $\vec{B} \parallel [110]$ we observe an effective g factor $g'_{\sigma,110}$ representing the splitting between the main σ^+- and σ^--polarized reflectance *minima*, which exhibits similar changes as $g'_{\sigma,100}$.

We observe

$$g'_{\sigma,110} = \begin{cases} -0.7 \text{ at } 1 \text{ T} \\ -0.9 \quad \text{for } B > 5 \text{ T} \end{cases} \tag{4.6}$$

and derive

$$g_{\sigma,110} = -1.3 \pm 0.2\,. \tag{4.7}$$

Equations (4.1), (4.2), and (4.5) yield the g values g_c, $\tilde{\kappa}$, and $\tilde{q}$, and, in particular, yield $\tilde{q} = -0.03$. If the experimental results obtained for $\vec{B} \parallel [110]$ are also taken into account, a somewhat smaller value for $\tilde{q}$ is suggested. Best overall agreement is obtained with the following set of g values:

$$g_c = -0.6 \pm 0.3\,, \tag{4.8}$$

$$\tilde{\kappa} = -0.1 \pm 0.1\,, \tag{4.9}$$

$$\tilde{q} = -0.02 \begin{cases} +0.01 \\ -0.02\,. \end{cases} \tag{4.10}$$

Experimentally measured σ^+-polarized reflectance spectra for $\vec{B} \parallel [110]$ at $B = 12$ and 18 T are shown in Fig. 3. Theoretical curves are also included. These are calculated for 1:3 relative oscillator strength of the two transitions. For the broken curves (including spatial dispersion) we use translational exciton masses $M_{1/2,110} = 0.31 m_0$ and $M_{3/2,110} = 0.97 m_0$ for the light- and heavy-hole bands, respectively, calculated according to Ref. 20. For $\vec{B} \parallel [100]$ the lower-energy reflectance structure is slightly broader than for $\vec{B} \parallel [110]$. This is attributed to inferior quality of the polished (100) surfaces compared to the cleaved (110) surfaces.

Reflectance spectra for $\vec{B} \parallel [110]$, Voigt configuration, and π polarization are shown in Fig. 4 for $B = 12$ and 18 T. The interesting feature of these spectra is the occurrence of a third transition in addition to the $|\frac{1}{2}\rangle\beta$ and $|-\frac{1}{2}\rangle\alpha$

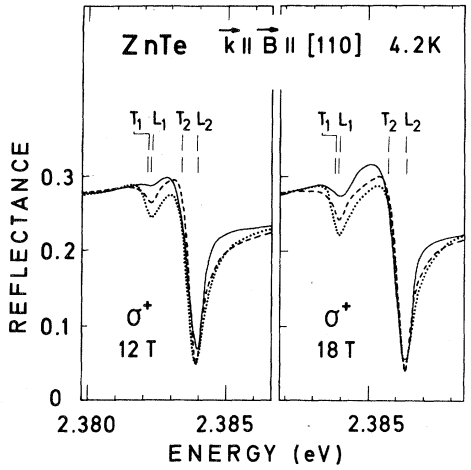

FIG. 3. Normal-incidence reflectance in Faraday configuration and σ^+ polarization for $\vec{B} \parallel [110]$, $B = 12$, 18 T. Solid lines: experimental spectra. Broken lines: theoretical calculation *including* spatial dispersion (SD). Dotted lines: theoretical calculation *neglecting* SD. T, L: energies of transverse and longitudinal exciton states. Upper labels (T_i, L_i) obtained considering SD, lower labels without SD. Absolute reflectance calculated. 1:3 relative oscillator strengths, other parameters see text.

states. As already mentioned in Sec. III A the reflectance curves with three oscillators are calculated without spatial dispersion. Parameters for the calculation are: background dielectric constant $\epsilon_b = 9.9$, 150-Å exciton-free layer, damping constant $\Gamma = 0.5$ meV, and $\beta_1:\beta_2:\beta_3 = 0.45:0.45:0.09$ relative oscillator strength for the transitions.

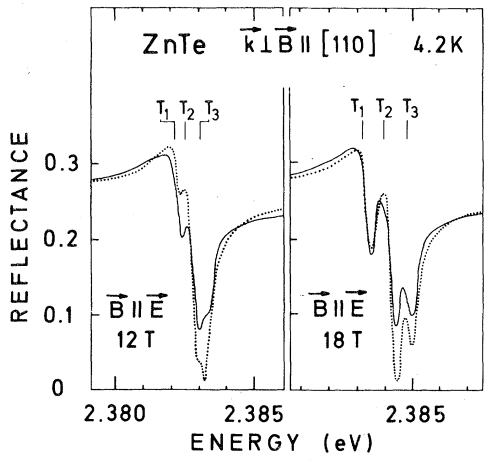

FIG. 4. Normal-incidence reflectance in Voigt configuration and π polarization for $\vec{B} \parallel [110]$, $B = 12$, 18 T. Solid lines: experimental spectra. Dotted lines: theoretical calculation *neglecting* spatial dispersion. T_1, T_2, T_3: energies of transverse exciton states. Absolute reflectance calculated. 0.45: 0.45: 0.09 relative oscillator strengths.

A comparison between the experimentally determined energy positions of the exciton sublevels and those calculated theoretically will be postponed to Sec. IV E. In addition to the g values the calculation requires as input parameters the exciton reduced mass μ_0 and the valence-band parameters γ_2^* and γ_3^*, which are derived in the following sections.

C. Exciton reduced mass

The exciton reduced mass μ_0 will be deduced in the following from the exciton Rydberg energy R_0^*. Reflectance measurements reveal a structure ~8 meV above the free-exciton ground state. This structure was already reported in Ref. 21 and attributed to the FE 2S state. The experimental observation is confirmed in the present investigation. However, the conclusion $\Delta E(1S - 2S) \simeq 8$ meV, where $\Delta E(1S - 2S)$ is the energy separation between the free exciton 1S and 2S states, is revised, since absorption data clearly demonstrate $\Delta E(1S - 2S) > 8$ meV.[4] The structure observed ~8 meV above the FE ground state is most likely related to the FE 2S state; however, we cannot give an explanation for the apparent energy shift compared to absorption. We take

$$R_0^* = 12.8 \pm 0.3 \text{ meV} \tag{4.11}$$

from Ref. 22, which was derived from $\Delta E(1S - 2S) = 9.8$ meV according to Ref. 23 and taking into account the valence-band parameters derived below.

According to Eq. (3.1a) the result obtained for μ_0^* from R_0^* depends critically on ϵ. Values reported in the literature for ϵ_0 vary considerably as the compilation in Ref. 24 shows. We use

$$\epsilon = 9.3 . \tag{4.12}$$

This value for ϵ characterizes the shallow (effective-mass) donor 1S-2S state energy separation as well as the 2S-3S state energy separation, which were measured on the samples under investigation here by excitation spectroscopy on donor acceptor pair transitions.[4] The FE binding energy is in between the donor 1S and 2S state binding energies, which are 18.3 and 4.6 meV, respectively.[4] Thus we consider the result derived from the effective-mass donor levels appropriate for the FE ground state also.

Equations (3.1a), (4.11), and (4.12) directly yield

$$\mu_0^* \text{ (EM)}/m_0 = 0.081 \pm 0.004 , \tag{4.13}$$

where (EM) indicates that the result is obtained

within the simple effective-mass theory.

Alternatively we derive the bare exciton reduced mass μ_0 from R_0^* using the results of Kane's variational calculation of exciton polarons.[25] Input parameters are the bare electron mass m_e, and the static and high-frequency dielectric constants, ϵ_0 and ϵ_∞, respectively. A rapidly converging iteration procedure based on the functions tabulated in Ref. 25 yields the bare exciton reduced mass and a hole mass, which is equivalent to $1/\gamma_1$ for degenerate valence bands. We did the iteration using $m_e = 0.111 m_0$ (equivalent to the polaron mass $m_e^* = 0.116 m_0$ given in Ref. 26), $\epsilon_0 = 9.3$, and $\epsilon_\infty = 6.9$. The latter value $\epsilon_\infty = 6.9$ is calculated from ϵ_0 by the Lyddane-Sachs-Teller relation and $\hbar\omega(\mathrm{TO}) = 22.5$ meV and $\hbar\omega(\mathrm{LO}) = 26.1$ meV.[4,27] The exciton reduced mass obtained is

$$\mu_0\ (\mathrm{Kane})/m_0 = 0.073 \pm 0.004\,, \tag{4.14}$$

where (Kane) indicates that the result is derived on the basis of Kane's calculation. Equation (4.14) represents the bare exciton reduced mass, and for comparison with Eq. (4.13) the corresponding polaron mass has to be evaluated. We derive μ_0^* from μ_0 by transforming m_e and γ_1 separately into the corresponding polaron values, since $r_{\mathrm{el}}^{\mathrm{pol}} + r_{\mathrm{hole}}^{\mathrm{pol}} \simeq r_{\mathrm{exc}}$, where $r_{\mathrm{el}}^{\mathrm{pol}}$ and $r_{\mathrm{hole}}^{\mathrm{pol}}$ are the electron and hole polaron radii, respectively, and r_{exc} is the free-exciton Bohr radius.

According to Ref. 14 we calculate

$$\gamma_1/\gamma_1^* = 1.12 \tag{4.15}$$

and using also the bare and renormalized electron masses as given in Ref. 26 (see above) we derive

$$\mu_0^*\ (\mathrm{Kane})/m_0 = 0.079 \pm 0.004\,. \tag{4.16}$$

This result is in good agreement with Eq. (4.13). Taking the average of Eqs. (4.13) and (4.16) we get

$$\mu_0^*/m_0 = 0.080 \pm 0.005$$

and (4.17)

$$\mu_0/m_0 = 0.074 \pm 0.005\,.$$

The values of the exciton reduced mass given in Eq. (4.17) are equivalent to

$$\gamma_1^* = 3.9 \pm 0.7$$

and (4.18)

$$\gamma_1 = 4.4 \pm 0.7\,,$$

The relatively large error for γ_1 is mainly due to the fact that $1/m_e$ is considerably larger than γ_1.

The exciton diamagnetic shift is essentially determined by the parameters μ_0^* and R_0^*. We use the results for μ_0^* and R_0^* for a comparison between experimental results and theoretical curves calculated on the basis of different models. This is shown in Fig. 5. Crosses represent experimental data. Curve 1 is the excitonic diamagnetic shift in the low-field limit according to Ref. 5 and calculated with *bare* parameters. Curve 2 is obtained by multiplication of curve 1 with a correction function $F(\gamma) = \Delta E_{\mathrm{dia}}(\gamma)/\frac{1}{2}\gamma^2 R_0$, where $\Delta E_{\mathrm{dia}}(\gamma)$ is the diamagnetic shift of an exciton determined in a two-band model variational calculation valid for $\gamma \lesssim 1$ *without* polaron correction. This calculation is equivalent to that performed by Cabib *et al.*[10] If the variational calculation is performed *including* polaron effects as outlined in detail in Ref. 7, we get the correction function $F^*(\gamma)$ [cf. Eq. (3.2)] and multiplication of curve 1 with $F^*(\gamma)$ yields curve 3. Finally, curve 1* is calculated according to the low-field three-band formula of Ref. 5 using *renormalized* parameters (instead of the *bare* parameters giving curve 1). Correction of curve 1* according to Ref. 10 yields results which are *not* included in Fig. 5, since they differ less than 3% from curve 3.

Curve 1* was calculated using $R_0^* = 12.8$ meV and $\mu_0^*/m_0 = 0.081$. The corresponding reduced bare exciton mass $\mu_0/m_0 = 0.076$ and $R_0 = 11.9$

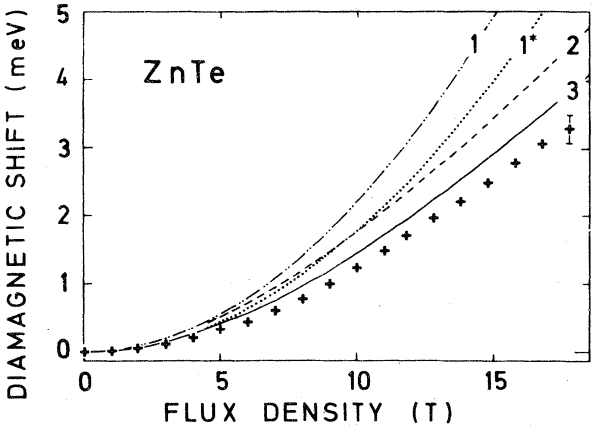

FIG. 5. Mean free-exciton diamagnetic shift (DS) rate. +: experimental results. Curve 1 (dash-dotted): DS according to low-field theory, calculated with *bare* parameters. Curve 2 (dashed): as curve 1, but corrected for finite γ, *neglecting* polaron effects. Curve 3 (solid): as curve 1, but corrected for finite γ *including* polaron effects. Curve 1* (dotted): DS according to low-field theory, calculated with *renormalized* parameters. Input parameters: $\epsilon_0 = 9.3$, $\epsilon_\infty = 6.9$, $\hbar\omega$ (LO) = 26.1 meV, $m_e^* = 0.116 m_0$; for curves 1, 2, 3: $R_0 = 11.9$ meV, $\mu_0 = 0.076 m_0$, corresponding renormalized parameters for curve 1*: $R_0^* = 12.8$ meV, $\mu_0^* = 0.081 m_0$. For references see text.

meV were taken as input parameters to calculate curves 1, 2, and 3.

The difference between curve 3 and the experimental results represents the discrepancy between experiment and the most adequate theory available at present (i.e., low-field theory for degenerate valence bands modified for $\gamma \lesssim 1$ and for polaron effects). Agreement between experiment and theory can be obtained assuming a hole mass $m_h = 0.29 m_0$ (cf. Fig. 2 of Ref. 28). The hole mass $m_h = 0.29 m_0$ corresponds to $\gamma_1 = 3.44$ and $\mu_0 = 0.080 m_0$. The difference between these values and those given in Eqs. (4.17) and (4.18) is nearly within the error limits, taking into account the error of the experimentally determined diamagnetic shift rate and also the error of the input parameters for the variational calculation. Thus we conclude that our theoretical approach to the diamagnetic shift is reasonable, although it is expected that the existing difference of ~10% between theory and experiment could be reduced by a more rigorous theoretical treatment.

D. Valence-band parameters γ_2 and γ_3

The ratio γ_2^*/γ_3^* is determined from the difference between the mean diamagnetic shift rate observed for $\vec{B} \parallel [100]$ and $\vec{B} \parallel [110]$ according to Eq. (3.11). The experiments yield

$$[\Delta E^-_{dia}(110) - \Delta E^-_{dia}(100)]/\Delta E^-_{dia}(100) = 0.42 \pm 0.03 , \quad (4.19)$$

and we derive

$$\gamma_2^*/\gamma_3^* = 0.64 \pm 0.04 , \quad (4.20)$$

neglecting the correction due to the k linear contribution [cf. Eq. (3.11)]. An exact value for the k linear coefficient K_1 of ZnTe is not available at present. However, K_1 has been determined experimentally for CdS ($\hbar K_1 = 0.5 \times 10^{-9}$ eV cm, Ref. 29) and for ZnO ($\hbar K_1 = 0.2 \times 10^{-9}$ eV cm, Ref. 30). There is no reason to assume a significantly larger value for ZnTe. Taking $\hbar K_1 = 0.5 \times 10^{-9}$ eV cm would increase the result for γ_2^*/γ_3^* by less than 0.01, and therefore we have omitted k-linear-dependent corrections.

The valence-band parameter γ_2^* is derived from the difference between the diamagnetic shift rates ΔE^σ_{dia} and ΔE^π_{dia} according to Eq. (3.12), valid for $\vec{B} \parallel [100]$. We measure

$$(\Delta E^\sigma_{dia} - \Delta E^\pi_{dia})/(\Delta E^\sigma_{dia} + \Delta E^\pi_{dia}) = 0.128 \pm 0.006 , \quad (4.21)$$

calculate $(\mu_0^* \gamma_2^*)$ as indicated in Sec. III D, and using Eqs. (4.17) and (4.20) we finally obtain

$$\gamma_2^* = 0.83 \pm 0.08 , \quad \gamma_2 = 0.95 \pm 0.09 , \quad (4.22)$$

$$\gamma_3^* = 1.30 \pm 0.12 , \quad \gamma_3 = 1.48 \pm 0.14 . \quad (4.23)$$

The renormalized parameters γ_i^* are those deduced from experiment; the bare parameters γ_i are calculated from γ_i^* according to Ref. 14.

E. Fan charts of exciton states

The magnetic-field-induced splitting and shift of the exciton substates depends on the parameters γ_i^*, μ_0^*, R_0^*, g_c, $\tilde{\kappa}$, and $\tilde{q}$. Using the numerical results of the present investigation we calculated the energy positions of the various exciton subcomponents. As already pointed out in Sec. IV C and shown in Fig. 5 we obtained the theoretical mean diamagnetic shift rate ~10% larger than measured experimentally. Owing to this difference comparison between experiment and theory with respect to relative shifts and splittings of the various subcomponents is more significant if the mean diamagnetic shift rate is subtracted. This has been done in Figs. 6 and 7, where theoretical and experimental results are shown for $\vec{B} \parallel [100]$ and $\vec{B} \parallel [110]$ and for σ^+, σ^-, and π polarization. The original experimental results are easily obtained adding the measured mean diamagnetic shift rate as shown in Fig. 5 to the experimental data points in Figs. 6 and 7.

Experimental results and theoretical curves for $\vec{B} \parallel [100]$ are shown in Fig. 6. The upper part (a) corresponds to Faraday configuration and the lower part (b) to Voigt configuration and π polarization. The theoretical curves are calculated according to Ref. 5 using renormalized parameters. Diamagnetic terms contributing to the

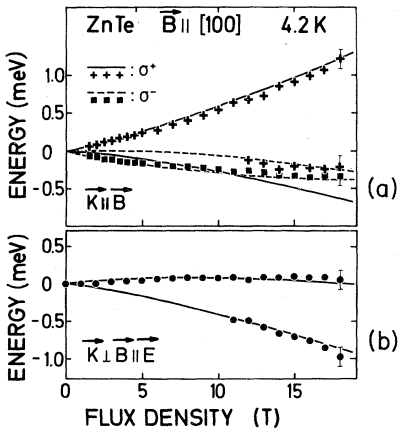

FIG. 6. Splitting of free-exciton subcomponents for $\vec{B} \parallel [100]$, mean diamagnetic shift subtracted. Solid and dashed lines: theory. Experimental: +, ■, ●. Identification of states in order of decreasing energy at high magnetic fields: (a): $|\tfrac{3}{2}\rangle\beta$, $|-\tfrac{1}{2}\rangle\beta$, $|-\tfrac{3}{2}\rangle\alpha$, $|\tfrac{1}{2}\rangle\alpha$; (b): $|\tfrac{1}{2}\rangle\beta$, $|-\tfrac{1}{2}\rangle\alpha$.

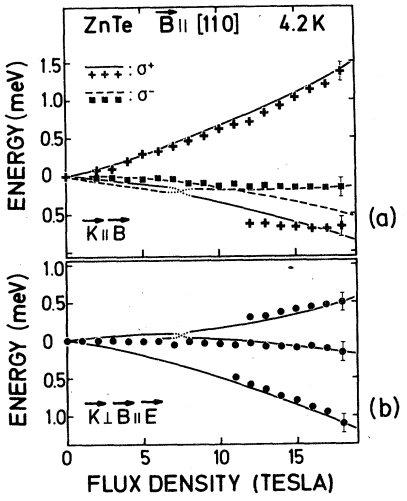

FIG. 7. Splitting of free-exciton subcomponents for $\vec{B}\|[110]$, mean diamagnetic shift subtracted. Solid and dashed lines: theory. Experimental: +, ■, ●. Predominant components of states in order of decreasing energy at high magnetic fields: (a): $|\frac{3}{2}\rangle\beta$, $|-\frac{3}{2}\rangle\alpha$, $|-\frac{1}{2}\rangle\alpha$, $|\frac{1}{2}\rangle\alpha$; (b) $|-\frac{3}{2}\rangle\beta$, $|\frac{1}{2}\rangle\beta$, $|-\frac{1}{2}\rangle\alpha$. Level crossing at 7–8 T indicated by dotted lines.

splitting are reduced by the ratio E/C, where E is the experimentally determined mean diamagnetic shift and C is the calculated diamagnetic shift as given by curve 1* in Fig. 5. This reduction is ~10% larger than according to the variational calculation, where the diamagnetic correction is given by the ratio (curve 3)/(curve 1*) of Fig. 5.

The various states in Fig. 6 are (going on the high-field side from high to low energies) $|\frac{3}{2}\rangle\beta$, $|-\frac{1}{2}\rangle\beta$, $|-\frac{3}{2}\rangle\alpha$, $|\frac{1}{2}\rangle\alpha$ for the σ states and $|\frac{1}{2}\rangle\beta$, $|-\frac{1}{2}\rangle\alpha$ for the π states.

The general agreement between experiment and theory is good. With respect to the low-energy σ^+-polarized $|\frac{1}{2}\rangle\alpha$ state there is a discrepancy beyond experimental error between experiment and theory. A similar result was already found in the case of ZnSe.[13] In that case the splitting between the two σ^--polarized states $|-\frac{3}{2}\rangle\alpha$ and $|-\frac{1}{2}\rangle\beta$ observed for $\vec{B}\|[100]$ was ~30% smaller than that calculated from a set of parameters which otherwise gave a very good representation of all exciton subcomponents reported in Ref. 13, and also of excited exciton states derived by two-photon absorption.[31] The mentioned discrepancy is expected to become smaller in a rigorous theoretical treatment, which is beyond the scope of the present paper.

A comparison between experiment and theory for $\vec{B}\|[110]$ is made in Fig. 7. The various states shown are $|\frac{3}{2}\rangle\beta$, $|-\frac{3}{2}\rangle\alpha$, $|-\frac{1}{2}\rangle\beta$, $|\frac{1}{2}\rangle\alpha$ for σ polarization and $|-\frac{3}{2}\rangle\beta$, $|\frac{1}{2}\rangle\beta$, $|-\frac{1}{2}\rangle\alpha$ for π polarization. For σ and π polarization a level crossing occurs at ~7–8 T where the states involved are strongly mixed. The curves representing the respective states are dotted.

The interesting difference between the results obtained for $\vec{B}\|[100]$ and $\vec{B}\|[110]$ is the pronounced appearance of a third structure in Voigt configuration and π polarization. According to the matrix (3.10) there is a mixing between the $|\frac{1}{2}\rangle\beta$ and $|-\frac{3}{2}\rangle\beta$ states and also between the $|-\frac{1}{2}\rangle\alpha$ and $|\frac{3}{2}\rangle\alpha$ states, induced by the off-diagonal elements in the matrix (3.10). The mixing between the dipole-allowed $|\frac{1}{2}\rangle\beta$ and the dipole-forbidden $|-\frac{3}{2}\rangle\beta$ states is sufficiently strong for the $|-\frac{3}{2}\rangle\beta$ state to become observable.

Concerning the energy position of the states the agreement between theory and experiment is good. However, for the $|-\frac{3}{2}\rangle\beta$ state we calculate only ~2% of the total π-polarized oscillator strength at 18 T, while the analysis of the measured reflectance curves yields almost 10%. The input parameters for the calculation cannot be varied in such a way that we get agreement with respect to relative oscillator strengths and simultaneously preserve reasonable relative energy separations. Consideration of k linear effects according to Ref. 2 did also fail to give an oscillator strength for the $|-\frac{3}{2}\rangle\beta$ state in agreement with experiment. Thus this discrepancy cannot be explained at present.

V. DISCUSSION

A consistency check for a set of valence-band parameters and the hole g value κ is provided by the expression[32,33]

$$\kappa = \gamma_3 + \tfrac{2}{3}\gamma_2 - \tfrac{1}{3}\gamma_1 - \tfrac{2}{3} \tag{5.1}$$

which holds for the bare (Luttinger) valence-band parameters. Using the results given in Eqs. (4.18), (4.22), and (4.23) we calculate $\kappa = 0.0_2$ from Eq. (5.1). On the other hand we derive $\kappa = -0.0_4$ from $\tilde{\kappa} = -0.1$ according to Eq. (3.1d). Both results are apparently in close agreement.

The electron g factor $g_c = -0.6$ derived here is in agreement with $g_c = -0.5_7$ derived in a previous analysis of similar but less detailed magnetoreflectance data.[21] From the magnetic-field-induced splitting of the Cu-acceptor bound exciton Dean and co-workers[34] determined $g_c = -0.38 \pm 0.05$, Toms *et al.*[35] derived an almost identical result $|g_c| = 0.39$ from spin-flip scattering of photoexcited conduction-band electrons, and very recent spin-flip measurements by Oka[36] yield $|g_c| = 0.41$. A somewhat smaller, however, less accurate result, $g_c = -0.15 \pm 0.15$, was derived from the spin splitting of the free-elec-

tron-to-acceptor (FB) transition.[26]

Taking into accout the experimental error of the various experimental results the agreement between the present g value and that obtained by other methods is considered satisfactory.

Lawaetz[37] calculated $g_c = +0.44$ in a five-band $\vec{k} \cdot \vec{p}$ analysis. The discrepancy between this value and the experimental results is fairly large. It is attributed to the influence of higher bands, which appears to be larger than assumed before. A similar conclusion was suggested by the difference between the calculated electron effective mass ($m_e = 0.18 m_0$, Ref. 37) and the experimental results ($m_e^* = 0.116 m_0$, Ref. 26 and $m_e^* = 0.122 m_0$, Ref. 38).

Valence-band parameters of ZnTe have been determined earlier by Lawaetz[37] (theoretical calculation) and by Stradling[39] (cyclotron resonance) and only recently from a theoretical fit to excited acceptor states by Herbert and co-workers[3] and also by Nakashima and co-workers.[40] Nakashima *et al.*[40] analyzed the $2S$ and $2P_{3/2}$ states of the As, P, and Li acceptors along the lines of the effective-mass treatment outlined in Ref. 23, while Herbert *et al.*[3] did a similar analysis of S-state series, $2P_{3/2}$ and $2P_{5/2}$ (Γ_8) states of the Cu, Li, and P acceptor (labeled *a*, *b*, and *e* acceptor in Ref. 3). The results of the different authors are compiled in Table I. Lawaetz states that his parameters are bare relative to the long-range interaction that couples the carriers to the polarization associated with long-wavelength optical vibrations in ionic crystals. However, Lawaetz uses input parameters taken from experiment which are, in general, polaron values. Consequently we do not consider the results as really "bare" and compare Lawaetz's data in Table I with renormalized parameters.

The agreement between the present results and those of Ref. 3 is excellent, and it is also good with respect to the results of Nakashima *et al.* Stradling's results differ from the present data and also from those found by all other authors by a relatively large value of γ_2^* compared to γ_3^*. Recent resonance Raman scattering data of exci-

TABLE I. Fundamental parameters of ZnTe.

Parameters	Present work	Results of other authors			
E_{1s} (free exciton)	13.2 ± 0.3 meV[a]				
R_0^*	12.8 ± 0.3 meV[a]				
μ_0^*/m_0	0.080 ± 0.005				
γ_1^*	3.9 ± 0.7	3.74[b]	4.00[c]	3.8[d]	4.2[e]
γ_2^*	0.83 ± 0.08	1.07[b]	1.15[c]	0.83[d]	0.91[e]
γ_3^*	1.30 ± 0.12	1.64[b]	1.29[c]	1.28[d]	1.54[e]
μ_0/m_0	0.074 ± 0.005				
γ_1	4.4 ± 0.7				
γ_2	0.95 ± 0.09				
γ_3	1.48 ± 0.14				
g_c	−0.6 ± 0.3	0.44[b]	−0.38[f]	−0.39[g]	−0.15[h]
$\tilde{\kappa}$	−0.1 ± 0.1				
$\tilde{q}$	$-0.02\,{}^{+0.01}_{-0.02}$				
κ	$-0.0_4 \pm 0.1$	0.42[b]			
q	$0.05\,{}^{+0.01}_{-0.02}$	0.05[b]			

[a] Reference 22.
[b] Reference 37.
[c] Reference 39.
[d] Reference 3.
[e] Reference 40.
[f] Reference 34.
[g] Reference 35 sign of g_c not given.
[h] Reference 26.

tonic polaritons by LO and acoustic phonons (Ref. 41) has been analyzed on the basis of Stradling's valence-band parameters. Agreement between experiment and theory was found in Ref. 41; however, the results are not very sensitive to γ_2^*. Accordingly, these experiments do not favor one result for γ_2^* compared to another. On the other hand, Lawaetz calculated a considerably smaller value of γ_1^* than found in the present investigation, but all other authors derived a value for γ_1^* close to that obtained here.

Finally, we calculate effective g factors for light and heavy holes according to Ref. 42, using the valence-band parameters and the hole g factor given above. In the spherical approximation we obtain $g_{1h}=1.0$ and $g_{hh}=2.5$, where both g values correspond to the lowest respective Landau levels. The result for g_{1h} is in good agreement with $0.9 \leq g_{1h} \leq 1.1$ found experimentally by spin-flip measurements.[43] The heavy-hole g value g_{hh} has not yet been measured.

VI. CONCLUSION

We have investigated the ground-state subcomponents of the free exciton in ZnTe in magnetic fields up to 18 T. Existing low-field theories for degenerate valence bands provide an adequate description of the experiments, if diamagnetic terms are reduced. The correction is determined in a two-band model variational calculation valid for polar materials and up to $\gamma \simeq 1$. Almost identical results (less than 3% deviation) are obtained if the analysis is performed with renormalized (polaron) parameters and diamagnetic terms are further corrected according to the variational calculation of Cabib *et al.*[10] A discrepancy of ~10% between theoretically and experimentally determined diamagnetic shift rates is attributed partly to experimental error and partly to shortcomings of our theoretical model.

We derive the electron and hole g factors, the exciton reduced mass, and a set of valence-band parameters γ_i. Our data provide a good overall representation of all exciton subcomponents observed.

ACKNOWLEDGMENTS

The authors are indebted to J. C. Pfister and B. Schaub of Centre d'Etudes Nucléaires de Grenoble (CENG) for providing high-purity ZnTe crystals, to the members of the Max-Planck-Institut für Festkörperforschung in the High-Magnetic-field Laboratory (HML, Grenoble) for their hospitality, to H. Hirt and P. Wurster for technical assistance, to G. Behnke for performing variational calculations, and to J. Lagois and K. Cho for making available computer programs for the calculation of reflectance curves and exciton splittings in magnetic fields.

---

*Present address: Siemens AG, FL OHL D 8000 München 83, West Germany.

†Present address: Centre National d'Etudes des Télécommunications, F 92220 Bagneux, France.

[1] D. Bimberg, in *Advances in Solid State Physics*, edited by J. Treusch (Vieweg/Pergamon, Braunschweig, 1977), Vol. XVII, p. 195.

[2] K. Cho, W. Dreybrodt, P. Hiesinger, S. Suga, and F. Willmann, in *Proceedings of the Twelfth International Conference on the Physics of Semiconductors, Stuttgart, 1974*, edited by M. H. Pilkuhn (Teubner, Stuttgart, 1974), p. 945.

[3] D. C. Herbert, P. J. Dean, H. Venghaus, and J. C. Pfister, J. Phys. C 11, 3641 (1978).

[4] H. Venghaus and P. J. Dean, Phys. Rev. B 21, 1596 (1980).

[5] K. Cho, S. Suga, W. Dreybrodt, and F. Willmann, Phys. Rev. B 11, 1512 (1975); 12, 1608 (1975).

[6] M. Altarelli and N. O. Lipari, Phys. Rev. B 7, 3798 (1973).

[7] G. Behnke, H. Büttner, and J. Pollmann, Solid State Commun. 20, 873 (1976).

[8] W. Ekardt, Phys. Status Solidi B 84, 293 (1977).

[9] F. Willmann, S. Suga, W. Dreybrodt, and K. Cho, Solid State Commun. 14, 783 (1974).

[10] D. Cabib, E. Fabri, and G. Fiorio, Nuovo Cimento B10, 185 (1972).

[11] B. Katircioglu, J. L. Pautrat, D. Bensahel, and N. Magnea, Radiat. Eff. 37, 183 (1978).

[12] J. Lagois, Phys. Rev. B 16, 1699 (1977).

[13] H. Venghaus, Phys. Rev. B 19, 3071 (1979).

[14] H. R. Trebin and U. Rössler, Phys. Status Solidi B 70, 717 (1975); H. R. Trebin, *ibid.* 81, 527 (1977); H. R. Trebin, Ph. D. thesis, University of Regensburg, Federal Republic of Germany, 1976 (unpublished).

[15] W. Ekardt, K. Lösch, and D. Bimberg, Phys. Rev. B 20, 3303 (1979).

[16] W. Wardzyński, W. Giriat, H. Szymczak, and R. Kowalczyk, Phys. Status Solidi B 49, 71 (1972).

[17] W. Wardzyński and M. Suffczyński, Solid State Commun. 10, 417 (1972).

[18] D. T. F. Marple, J. Appl. Phys. 35, 539 (1964).

[19] D. Berlincourt, H. Jaffe, and L. R. Shiozawa, Phys. Rev. 129, 1009 (1963).

[20] E. O. Kane, Phys. Rev. B 11, 3850 (1975).

[21] H. Venghaus, P. J. Dean, P. E. Simmonds, J. Lagois, and D. Bimberg, Solid State Commun. 24, 5 (1977).

[22] H. Venghaus and P. J. Dean, Solid State Commun. 31, 897 (1979).

[23] A. Baldereschi and N. O. Lipari, Phys. Rev. B 8, 2697 (1973); 9, 1525 (1974).

[24] K. Kunc, Ann. Phys. (N.Y.) 8, 319 (1973/74).

[25]E. O. Kane, Phys. Rev. B 18, 6849 (1978).
[26]P. J. Dean, H. Venghaus, and P. E. Simmonds, Phys. Rev. B 18, 6813 (1978).
[27]H. Venghaus, P. J. Dean, P. E. Simmonds, and J. C. Pfister, Z. Phys. B30, 125 (1978).
[28]H. Venghaus, B. Jusserand, and G. Behnke, Solid State Commun. 33, 371 (1980).
[29]G. D. Mahan and J. J. Hopfield, Phys. Rev. 135, A428 (1964).
[30]K. Hümmer, R. Helbig, and M. Baumgärtner, Phys. Status Solidi B 86, 527 (1978).
[31]M. Sondergeld, Phys. Status Solidi B 81, 253 (1977); 81, 451 (1977).
[32]G. Dresselhaus, A. F. Kip, and C. Kittel, Phys. Rev. 98, 368 (1955).
[33]R. L. Aggarwal, in *Semiconductors and Semimetals*, edited by R. K. Willardson and A. C. Beer (Academic, New York, 1972), Vol. 9, p. 151.
[34]P. J. Dean, H. Venghaus, J. C. Pfister, B. Schaub, and J. Marine, J. Lumin. 16, 363 (1978).
[35]D. J. Toms, J. F. Scott, and S. Nakashima, Phys. Rev. B 19, 928 (1979).
[36]Y. Oka, private communication.
[37]P. Lawaetz, Phys. Rev. B 4, 3460 (1971).
[38]B. Clerjaud, A. Gélineau, D. Galland, and K. Saminadayar, Phys. Rev. B 19, 2056 (1979).
[39]R. A. Stradling, Solid State Commun. 6, 665 (1968).
[40]S. Nakashima, T. Hattori, P. E. Simmonds, and E. Amzallag, Phys. Rev. B 19, 3045 (1979).
[41]Y. Oka and M. Cardona, Solid State Commun. 30, 447 (1979).
[42]J. M. Luttinger, Phys. Rev. 102, 1030 (1956).
[43]R. L. Hollis and J. F. Scott, Phys. Rev. B 15, 942 (1977).